Ocean Systems Engineering, *Vol. 9, No. 4 (2019) 349-368*
DOI: https://doi.org/10.12989/ose.2019.9.4.349

Response of triceratops to impact forces: numerical investigations

Srinivasan Chandrasekaran* and R. Nagavinothini

Department of Ocean Engineering, IIT Madras, India

(Received March 18, 2019, Revised September 17, 2019, Accepted September 19, 2019)

Abstract. Triceratops is one of the new generations of offshore compliant platforms suitable for ultra-deepwater applications. Apart from environmental loads, the offshore structures are also susceptible to accidental loads. Due to the increase in the risk of collision between ships and offshore platforms, the accurate prediction of structural response under impact loads becomes necessary. This paper presents the numerical investigations of the impact response of the buoyant leg of triceratops usually designed as an orthogonally stiffened cylindrical shell with stringers and ring frames. The impact analysis of buoyant leg with a rectangularly shaped indenter is carried out using ANSYS explicit analysis solver under different impact load cases. The results show that the shell deformation increases with the increase in impact load, and the ring stiffeners hinder the shell damage from spreading in the longitudinal direction. The response of triceratops is then obtained through hydrodynamic response analysis carried out using ANSYS AQWA. From the results, it is observed that the impact load on single buoyant leg causes periodic vibration in the deck in the surge and pitch degrees of freedom. Since the impact response of the structure is highly affected by the geometric and material properties, numerical studies are also carried out by varying the strain rate, and the location of the indenter and the results are discussed.

Keywords: impact analysis; stiffened cylindrical shell; ring frames; stringers; triceratops

1. Introduction

In order to extend the oil exploration and production to greater water depths, structures with adaptable structural forms are necessary. Triceratops is one of the new generation offshore compliant platforms, consisting of a deck connected to three buoyant legs by ball joints (White *et al.* 2005). The ball joints restrain the transfer of rotational motion and allow only the translational motion between the deck and buoyant legs. The buoyant legs are position restrained by a set of taut moored tethers. These platforms are highly suitable for ultra-deep waters under different sea state conditions (Chandrasekaran and Nagavinothini 2018, Nagavinothini and Chandrasekaran 2019, Srinivasan Chandrasekaran and Nagavinothini 2019a, b). The conceptual design of triceratops is shown in Fig. 1. The buoyant legs are usually designed as orthogonally stiffened cylindrical shells with stringers and ring frames to resist the axial load and hydrostatic pressure. The buoyant legs also have a relatively high radius to thickness ratio. Due to the large distance

*Corresponding author, Professor, E-mail: drsekaran@iitm.ac.in

http://www.techno-press.org/?journal=ose&subpage=7 ISSN: 2093-6702 (Print), 2093-677X (Online)

from the shore, offshore ultra-deepwater structures like triceratops requires servicing from bigger supply boats and vessels. So, the buoyant legs in triceratops are prone to impact loads that may arise due to ship platform collision involving higher impact energy. As a result of such collision events, local or global deformations may occur in the buoyant leg, which may subsequently affect the total strength and stability of the whole platform. Also, the response of triceratops under accidental loadings highly depends upon the material and geometric properties of the structure. Thus, it is highly necessary to assess the collision resistance of triceratops against impacts for a sensible design without an increase in the total weight of the structure.

With the increase in the number of oil production and exploration platforms, the risk of ship collision and ice impact has also substantially grown in the recent past. The ship platform collision is a dynamic process, and it involves several dynamic factors such as the type of collision, contact interval of the collision, energy absorption, and dissipation, to assess the structural response (Kvitrud 2011). Though the collisions had not resulted in the loss of lives or personal injuries, the economic consequences have been significant. The compliance of floating rigs may even increase the risk involved in impacts, because of very little or even no redundancy in the structure. Also, the post-collapse strength of the main structural components of such platforms would be very low. A relatively small dent of very less thickness will reduce the design safety factor from the structural member.

The structural behavior of tubular members under impact loads has been investigated by many studies found in the literature. The tubular members are commonly used in fixed offshore platforms. Khedmati and Nazari studied the structural behavior of preloaded tubular members under impact loads through numerical investigations (Khedmati and Nazari 2012). Jin *et al*. presented a non-linear dynamic analysis procedure for determining the impact action based on forensic evidence from the damaged members. The barge impact is simulated with a triangle impulse load with different contact collision times (Jin *et al*. 2005). Ronald and Dowling studied the response of stiffened cylinders to accidental lateral loading. The damage is applied at the mid-span of the cylindrical shell by a knife edge indenter (Ronalds and Dowling 1988). Experimental and numerical studies carried out under low-velocity impact discussed the details of ring stiffeners on cylinders; studies presented the failure modes and an estimate of critical load (Cerik *et al.* 2015, Do *et al*. 2018, Feng *et al*. 2017). Experimental tests carried out on ring-stiffened cylinders, loaded at mid-span by a wedge-shaped indenter were in closer agreement with that of the detailed finite element analysis of a geometrically-identical specimen (Karroum *et al.* 2007). Storheim and Amdahl investigated the damage to the offshore platform under ship impacts. The ship-platform interaction was studied by modeling both structures using nonlinear finite element analysis. The collision forces were also compared with the standard force-deformation curves in the NORSOK code (Storheim and Amdahl 2014). Recent studies have also reported that the nonlinear finite element analysis under impact loading of structures requires exact material characteristics to avoid errors. The accuracy can be improved further by providing dynamic material properties. The strain rate effect should be considered to predict the impact response of the structure accurately. Though several studies and standard regulations give the impact results of unstiffened tubes and stiffened cylindrical shells, they cannot be directly applied to the present problem because of a large D/t ratio of buoyant legs.

In the given context, this paper describes the history of ship platform collisions in the recent past and the preliminary design of buoyant legs first. Then, the numerical analysis of a single buoyant leg modeled as an orthogonally stiffened cylindrical shell is attempted to evaluate the impact response of the structure, by modeling the vessels as a rigid rectangular box-shaped

indenter. As triceratops are one of the emerging new generation offshore compliant platforms, this study will be of paramount importance to validate the structural behavior of the platform under accidental impact loading. The dynamic material properties of marine steel are also taken into account in the numerical analysis. The response behavior and deformation pattern of buoyant leg under different shape, size, and location of the indenters are reserved for future studies. Also, the structural behavior under post failure of the buoyant leg is not taken into account. The methodology followed in the present study is shown in Fig. 2.

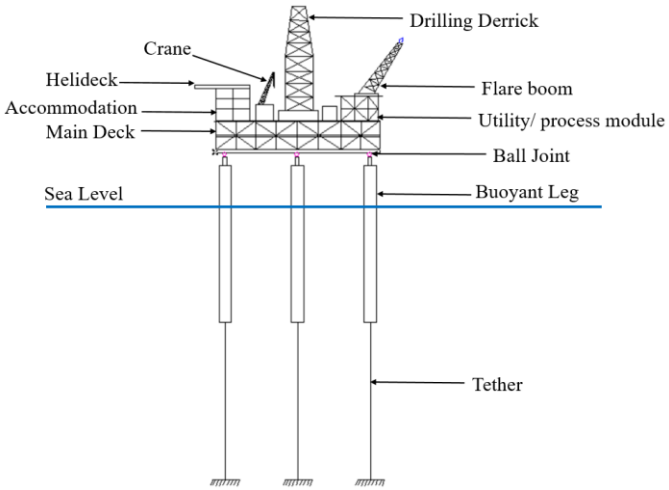

Fig. 1 Conceptual model of Triceratops

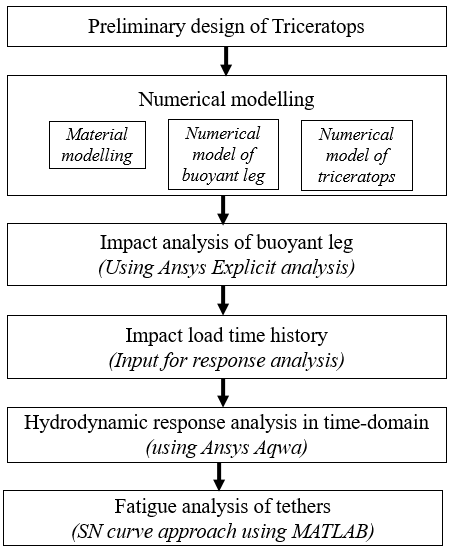

Fig. 2 Methodology of the present study

Table 1 Platform ship collisions

Platform	Vessel	Date	Mass of vessel	Speed of vessel (m/s)	Collision energy (MJ)
West venture semisubmersible	Far Symphony	7th March 2004	5000 tons	3.7	39
Ekofisk 2/4-P Jacket	Ocean carrier	2nd June 2005	4.679 deadweight tons	3	20
Njord B FSU	Navion Hispania	13th November, 2006	126.13 dead weight tons	1.2	61
Grane Jacket	Bourbon Surf	18Th June 2007	3.117 deadweight tons	1 - 3.5	Low
Ekofisk 2/4-P tripod Jacket	Big Orange XVIII	8th June 2009	6000 tons	4.5 – 4.8	70

2. Ship platform collision

In order to avoid the failure of offshore platforms due to accidental collisions, standard regulations and guidelines should be followed in the design of the structures prone to accidental impacts (Amdahl and Eberg 1993). Based on NORSOK N-003 guidelines for production platforms, 5000 tons supply ships with speed not less than 2m/s for design checks, should be considered for impact analysis (NORSOK standard N-003, 2007). Significant damage to the platform is allowed. However, the damage should not lead to the progressive collapse of the structure. The regulation of Norwegian Maritime Directorate together with DNV standards also suggests the requirement of a collision of 5000 tons ship at a speed of 2.0 m/s for the design of structures exposed to ship collisions. The most common colliding vessel in offshore locations are the supply boats. Based on the review of collision incidents, it was observed that the majority of collision events involved with energies of less than 0.5 MJ. Also, design guidelines suggest 4 MJ be the minimum collision energy for the design of structures under accidental events. Based on a statistical overview, a major number of collisions occurred with visiting vessels (Kvitrud 2011). It is also observed that the average displacement of the visiting vessels also increased by about 100 tons in the past 30 years. With the increased weight, the vessels are capable of causing more damage due to the increase in collision energy. The collision events that happened in the recent past are listed in Table 1. The recent collision events with greater collision energy and increased speed of the supply vessel indicate that the standard design collision event is under-represented.

The main concern of the present study is to investigate the response of buoyant legs under rigid rectangular indenters. A rectangular box-shaped indenter of length 10 m, breadth 5.0 m, depth 2.0 m, and 7500-ton displacement is considered as a striking mass representing the shipping stem, or so-called stem bar. Though the design guidelines suggest a vessel displacement of 5000 tonnes, the present study considers the vessels with higher displacement due to the increase in the size of vessels visiting offshore structures in ultra-deep waters in the recent years. The indenter impacts the cylindrical shell at the height of 5.0 m from the Mean Sea Level. The collision cases considered for the study are given in Table 2. The assumed load cases may be considered as the central sideways collision of the ship with the buoyant leg of a triceratops. The damage ultimately depends upon the energy absorbed by the platform. In this study, the indenter is assumed to be infinitely rigid, and the energy is dissipated only by the platform. Ductility design is followed, which implies that the platform dissipates a major part of collision energy by undergoing large

Table 2 Collision speed and impact duration (Syngellakis and Balaji 1989)

Case	Collision speed (m/s)	The impact duration (seconds)
Case 1	1.0	0.30
Case 2	2.0	0.35
Case 3	3.0	0.38
Case 4	4.0	0.40

plastic deformation (Storheim and Amdahl 2014). The shape of indenter determines the form of damage, and the assumption above can simplify the calculations.

3. Preliminary design of the buoyant leg

Since triceratops is in the developmental stage of design, the geometric form of triceratops for ultra-deep waters (water depth of 2400 m) is developed based on the dimensions of the Perdido spar platform (Liapis *et al*. 2010). The height and topside weight of the platform is maintained the same as that of the spar platform, and the spar hull buoyancy is equally distributed to three buoyant legs. The platform has a total buoyancy force of 821 MN. The outer diameter of each buoyant leg is 15.0 m. The total length of the buoyant leg is 174.24 m with a freeboard of 20.24 m.

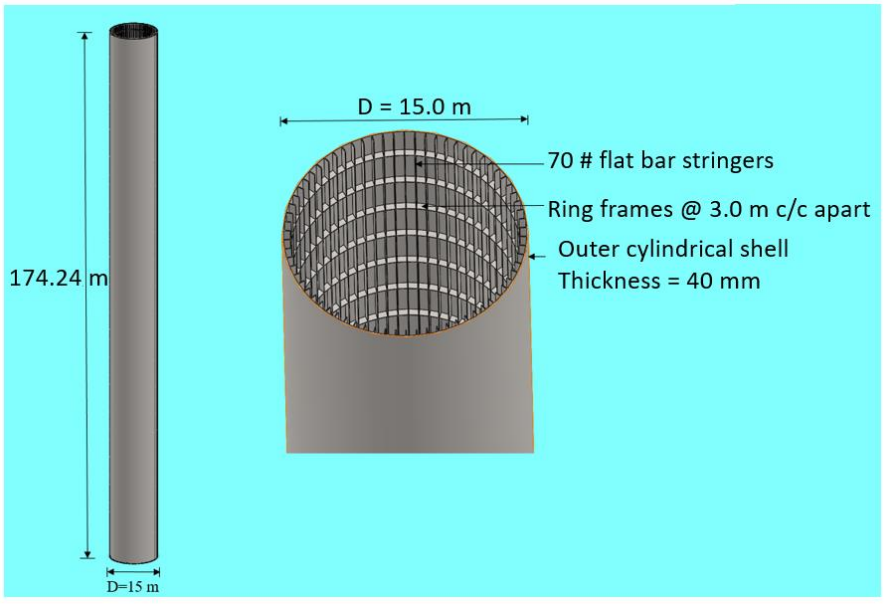

Fig. 3 Stiffened cylindrical shell and buoyant leg

Thin-walled cylindrical shells with orthogonal reinforcements such as ring frames and stringers are used as buoyant legs, as weight and buoyancy of triceratops is a major concern in design. The environmental condition used for the preliminary design of buoyant leg accounts for an intermediate environmental condition in the Gulf of Mexico (Significant wave height = 7.9 m, Peak period = 9.1 seconds). The thickness of the shell is 40 mm. The cylindrical shell is provided with 70 flat bar stringers (300 mm x 40 mm), and flat bar rings of the same dimension are provided along the length with 3m c/c spacing (Chandrasekaran and Nagavinothini 2018). Heavy ring frames are provided at the ends of the cylindrical shell. This condition ensures that the ends of the cylinder remain circular under loading. The conceptual model of the buoyant leg is shown in Fig. 3. The buckling behavior is the major factor affecting the design of orthogonally stiffened cylindrical shells. The buckling strength calculations are performed as per DNV standards (DNV-RP-C-202, 2010). The cylindrical shell is checked against shell buckling, panel ring buckling, column buckling, and combined buckling cases, and it is found that the design criterion is satisfied. Thought this method is considered semi-empirical, there is good agreement between the theoretical and experimental values, as mentioned in the literature.

4. Material properties

The innovative structural form, loading conditions, and material properties of buoyant legs make them different from other commonly used cylindrical shell structures. The difference in the material properties causes significant changes in the structural behavior of the cylindrical shells. The type of steel considered in this study is AH 36 marine steel. The mechanical properties of steel are given in Table 3. In the impact analysis, the material properties suggested by Cho *et al*. (2015) based on a large number of dynamic tensile tests are used. The true stress-strain values are calculated from the engineering stress-strain values by the following equations (Cho *et al.* 2015, Cerik *et al.* 2015)

$$\sigma_t = \sigma_{eng}(1+\varepsilon_{eng}) \tag{1}$$

$$\varepsilon_t = \ln(1+\varepsilon_{eng}) \tag{2}$$

Where, σ_t is the True stress, σ_{eng} is the engineering stress, ε_t is the true strain and ε_{eng} is the engineering strain. The static constitutive equation considering the yield plateau is given by

$$\sigma_t = E\varepsilon_t \qquad \text{when } 0 < \varepsilon_t \le \varepsilon_{Yt} \tag{3}$$

$$\sigma_t = \sigma_{Yt} + \left(\sigma_{HSt} - \sigma_{tY}\right)\left(\frac{\varepsilon_t - \varepsilon_{Yt}}{\varepsilon_{HSt} - \varepsilon_{Yt}}\right) \qquad \text{when } \varepsilon_{Yt} < \varepsilon_t \le \varepsilon_{HSt} \tag{4}$$

$$\sigma_t = \sigma_{HSt} + \left(\frac{\sigma_{Tt} - \sigma_{HSt}}{\left(\varepsilon_{Tt} - \varepsilon_{HSt}\right)^A}\right)\left(\varepsilon_t - \varepsilon_{HSt}\right)^A \quad \text{when } \varepsilon_{HSt} < \varepsilon_t \tag{5}$$

$$A = \frac{\sigma_{Tt}}{\sigma_{Tt} - \sigma_{HSt}}\left(\varepsilon_{Tt} - \varepsilon_{HSt}\right) \tag{6}$$

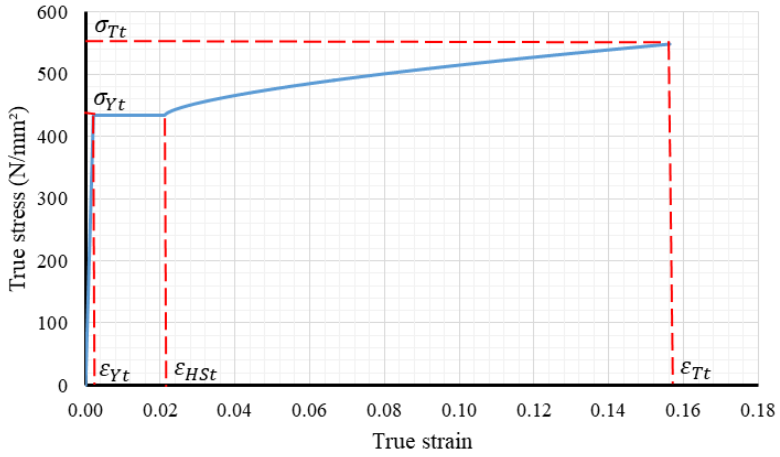

Fig. 4 True stress-strain curve of AH 36 grade steel

Table 3 Mechanical properties of Marine steel AH36 (Cho *et al.* 2015)

Mechanical properties	Value	Units
Yield Strength	433	N/mm^2
Young's modulus	206000	N/mm^2
Ultimate Tensile strength	547	N/mm^2
Ultimate Tensile Strain	0.156	No unit
Hardening start strain	0.0214	No unit

Where σ_{Yt} is the true yield stress, σ_{HSt} is the true hardening start to stress, σ_{Tt} is the true ultimate stress, ε_{Yt} is the true yield strain, ε_{HSt} is the true hardening starts to strain and ε_{Tt} is the true ultimate strain. The true stress-strain curve for AH36 steel, considering the yield plateau is shown in Fig. 4. This true stress-strain curve is used for the numerical analysis as they represent the state of the material more accurately. The same data is given as the input for defining the material plasticity in ANSYS. It should be noted that in the static constitutive equation used for developing the true stress-strain curve, the initial yield delay is neglected.

In order to predict the impact response of the structure more accurately, the strain-rate effect should be considered. It is highly important in impact analysis because the residual strength in damaged condition will be considered in the design against impact load (Cerik *et al.* 2015). When strain rate increases, yield delay occurs in the material before entering the yield plateau. The width of the yield plateau is also highly affected by the strain rate. In order to include the strain rate hardening effects of the material, the dynamic constitutive equations provided by Cho *et al*. (2015) are used. These equations for dynamic yield strength, dynamic ultimate tensile strength, dynamic hardening start strain, and dynamic ultimate tensile strain were developed based on the dynamic tensile tests

$$\sigma_{Yd} = 1 + \left\{ \left(\frac{E\sigma_T}{1000\sigma_Y^2} \right)^{4.89} \left(\frac{\dot{\varepsilon}}{233.6} \right) \right\}^{0.333} \tag{7}$$

$$\sigma_{Td} = \left(1 + 0.12\dot{\varepsilon}^{(-n)}\right)\sigma_{Yd} \tag{8}$$

$$\varepsilon_{HSd} = \left(1 + (p \times \dot{\varepsilon})^{0.3}\right)\varepsilon_{HS} \tag{9}$$

$$\varepsilon_{Td} = \left(1 + \frac{\dot{\varepsilon}}{q}\right)^{-0.333} \tag{10}$$

where

$$n = 11.14 \times \exp\left(\frac{138\sigma_Y}{\sigma_T}\right), \quad p = 10.2 \times \exp\left(-0.52\left(\frac{1000\sigma_Y}{E}\right)^{2.2}\left(\frac{\sigma_T}{\sigma_Y}\right)^{2.8}\right) \tag{11}$$

$$q = 4.71\left\{\left(\frac{1000\sigma_Y}{E}\right)^{8}\left(\frac{\sigma_T}{\sigma_Y}\right)^{0.3}\right\}^{2.08} \tag{12}$$

$\dot{\varepsilon}$ Is the strain rate, σ_{Yd} is the dynamic yield strength, σ_{Td} is the ultimate dynamic strength, ε_{HSd} is the dynamic hardening start to strain and ε_{Td} is the dynamic ultimate tensile strain.

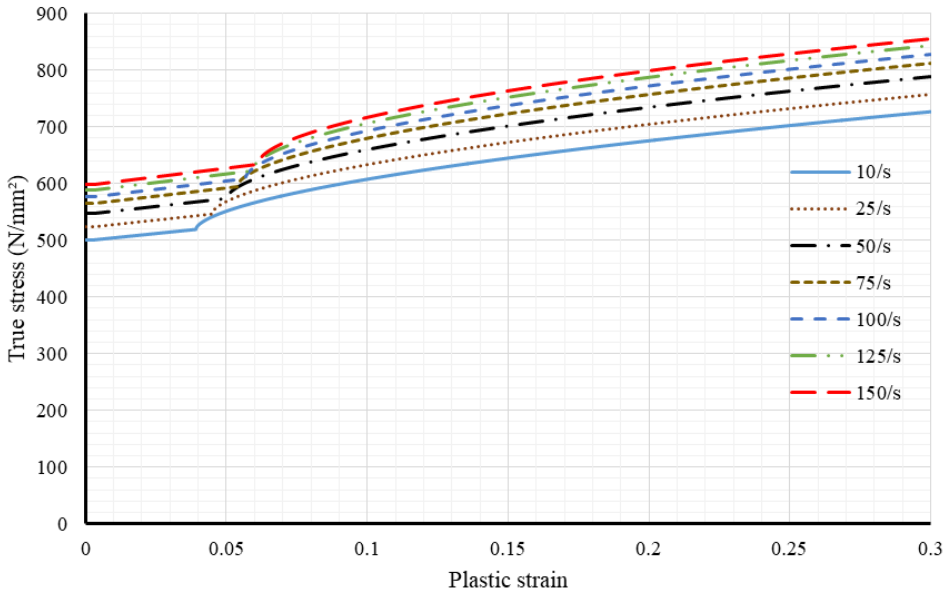

Fig. 5 True stress-plastic strain curve for different strain rates

From the dynamic constitutive equation, the true stress plastic curves are plotted for different strain rate values (10 s^{-1}, 25 s^{-1}, 50 s^{-1}, 75 s^{-1}, 100 s^{-1}, 125 s^{-1}, 150 s^{-1}) in Fig. 5. It can be seen that the initial yield and the width of the yield plateau increase with the increase in the strain rate. At higher strain rates, the effect of strain hardening reduces significantly. Also, the material behaves perfectly plastic under increased strain rate. It is to be noted that the above equations provide better results than Cowper-Symonds equation (Singh *et al.* 2011).

5. Numerical analysis

For numerical analysis of the buoyant leg, the outer cylindrical shell, stringers and ring frames are modeled as shell elements using Ansys Design Modeller with hourglass damping and central difference time integration scheme. The rectangular box-shaped indenter resembling the stem of the ship is modeled using solid elements, and it is assumed to be perfectly rigid without deformation. Thus, during impact strain, energy dissipation is confined to a cylindrical shell and the stiffeners. Impact analysis is carried out using Ansys Explicit Solver. The contact region is defined using the general body interactions option in the solver. The outer surface of the shell and the indenter surface are chosen as the contact surfaces. The Courant-Friedrichs-Lewy condition is followed to limit the time step used in the explicit analysis, in order to ensure stability and accuracy of the solution. The shell meshes with four-node quadrilateral shell elements. The nodes on the sides of the shell elements are connected by vertical lines. The indenter meshes with the regular meshing pattern. The quality of the solution is checked through momentum and energy conservation for different mesh sizes. The mesh size of 0.3 m is adequate in predicting the stress-strain relationship accurately. The discontinuities in the flow variables under shock waves due to strong impacts are handled by viscous terms in the solver. A quadratic artificial viscosity coefficient of 1 is used to avoid discontinuities, and a linear artificial viscosity coefficient of 0.2 is used to damp the oscillations in the solution. The viscous formulation is used to calculate the hourglass forces with a viscous coefficient of 0.1. The top and bottom ends of the cylindrical shell are restrained in all degrees of freedom.

The initial collision velocity of 5.0 m/s is applied to the rectangular indenter at 5.0 m above the Mean Sea Level (MSL) in the impact direction for the simulation of impact energy. The height of the impact location form the MSL is chosen based on the height of the vessels visiting the offshore structures, and the height of the impact location in the collision events reported earlier (Storheim and Amdahl 2014). The striking mass is restrained in all degrees of freedom except in the impact direction. The material plasticity data, as shown in Figs. 4 and 5 is defined using true stress equivalent plastic data obtained from the constitutive equations by using a multi-linear isotropic hardening model with Von-Mises failure criteria. It has been used subsequently in the numerical simulation. A schematic view of the cylindrical shell and the striking mass are shown in Fig. 6. The horizontal and vertical lines on the surface of the cylindrical shell are stringer and ring stiffeners, respectively. Previous studies reported that the predominant component of deformation is the local indentation at the initial stages of impact loading. The impact loads did not vary beyond the length of 30 m from MSL. In order to reduce the analysis run time and computational efforts, the results are obtained for a cylinder length of 45.26 m, shorter than the actual length of the buoyant leg with simply-supported ends which compensates for the increase of bending rigidity. After meshing, the whole model has 60140 nodes and 46048 elements, which considerably extended the run time.

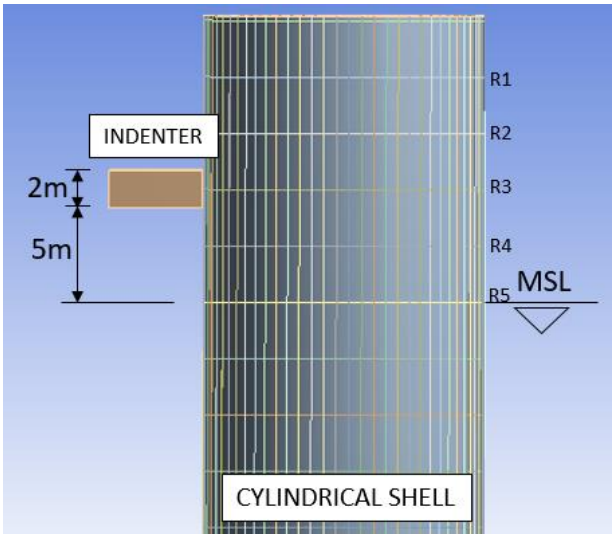

Fig. 6 Schematic view of striking mass and indenter

6. Numerical results and discussion

6.1 Damage profile

The impact location is on ring stiffener at 9.0 m from the top of the cylindrical shell. The indenter displacement along the direction of impact under different impact load cases are shown in Fig. 7. The impact causes a local dent leading to flattening of the cylindrical shell and ring stiffener at the impact location. The equivalent stress distribution of the cylindrical shell for different cases with 0.30s impact duration is shown in Fig. 8. The flattening of the local dent increases with the increase in the contact area of the indenter. The ring stiffeners hinder the damage spreading to the adjacent bay. Hence, it acts as an obstruction to circumferential bending (Do *et al*. 2018). The ring stiffener on the impact location alone undergoes maximum deformation, whereas the adjacent ring frames deformed only about 35% of maximum deformation. The ring frames at the end of the cylindrical shell remain circular unaffected by impact load. The plastic strain in the cylindrical shell is observed only within the adjacent bays of the deformed ring stiffener on impact location. The longitudinal stringer stiffeners between the ring stiffeners collapsed as a beam. With the increase in the dent depth at the impact location, the stringers adjacent to the damaged stringer starts deforming with the cylindrical shell. The local tripping of stiffeners is observed close to the deformed ring stiffener. Thus, it can be said that the stringers played an important role in resisting the impact load.

The same failure pattern is observed under an impact speed of 2 m/s with an increased impact duration. In this case, the maximum equivalent stress extends up to the top edge of the cylinder. However, the ring frames reduce the spread of plastic deformation to the adjacent bays from the impact location. The elastic strain is observed up to a depth of 6m from the Mean Sea level. Torsional twisting in the stringers is also observed very close to the ring stiffener on the impact location. The maximum plastic strain occurs at the ring stiffener at the impact location. With the

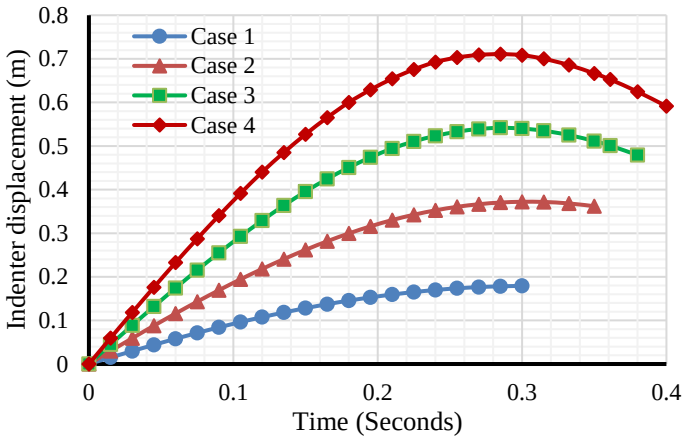

Fig. 7 Indenter displacement under different impact cases

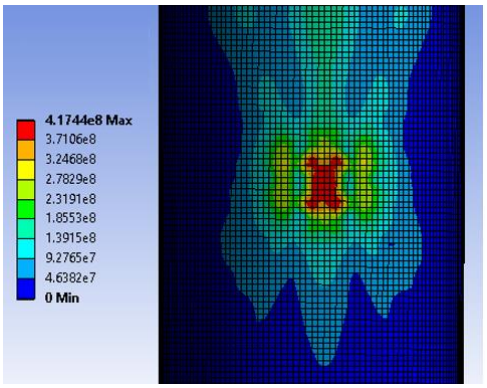

(a) Case 1

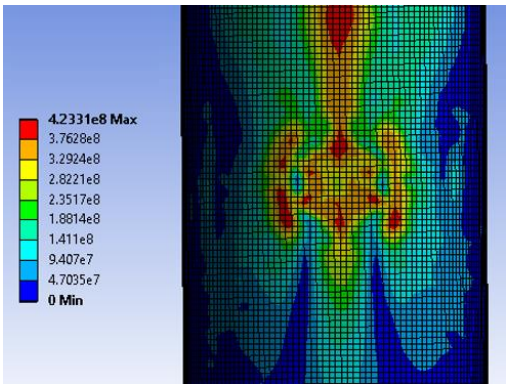

(b) Case 2

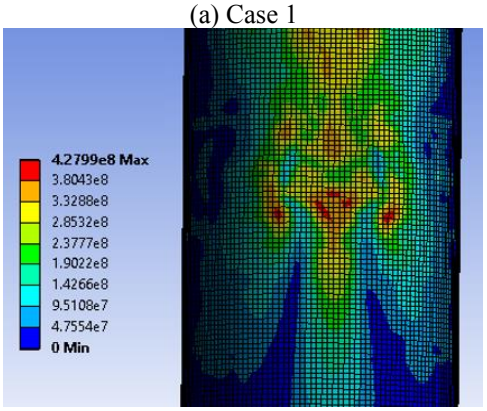

(c) Case 3

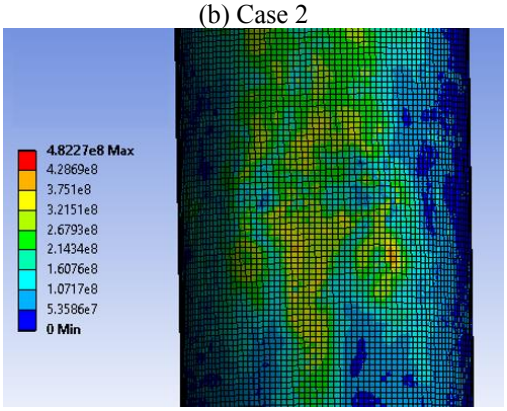

(d) Case 4

Fig. 8 Equivalent stress distribution of cylindrical shell

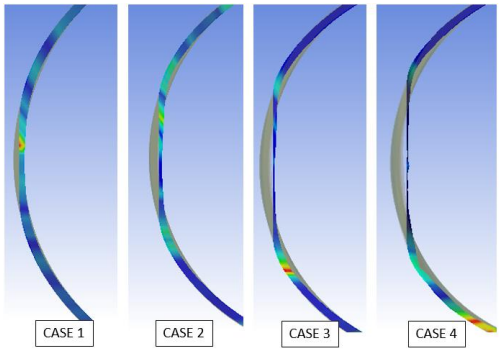

Fig. 9 Deformation of ring stiffener R3 at 6.0 m above MSL

increase in the impact velocity and impact duration, the maximum equivalent stress, and the deformation increases in the cylindrical shell. The principal stress in the cylindrical shell increases to a depth of 27.0 m from MSL. However, the plastic strain is observed only on the impact location. The cylindrical shell bulges out at the end of the flattened dent caused due to impact. The displacement of the shell along the direction of impact is about 0.5 m. Under case 4, the damage increases due to the increase in the contact area. The deformation pattern of ring stiffener, R3 at the impact location for all load cases are shown in Fig. 9. With the increase in the contact area, the flattening of the ring frames increases and stiffener bulges out from the ends of the flattened section along with the cylindrical shell. Since the center of impact of the indenter is on the ring stiffener, the maximum plastic strain under all load cases is seen on R3 ring stiffener only. In case 4, the area of damage is larger compared to other cases. The maximum stress is developed in the cylindrical shell only in case 4. The maximum stress developed in case 4 is 484 MPa, which is 13% higher than that of case 3.

6.2 Force-displacement characteristics

The results of important parameters from the impact analysis are summarized in Table 4. The peak force and deformation in buoyant leg increase with the increase in impact velocity and duration. The maximum energy absorbed by buoyant leg under case 4 is 6.279 MJ. The force versus non-dimensional displacement curves is shown in Fig. 10. The area under these curves gives the total energy absorbed by the buoyant leg for different impact load cases under consideration. As seen from the figure, the flattening of curves at a particular instant of time occurs due to torsional buckling of stiffeners. It can be said that the impact loads with higher intensity may lead to a local weakening of the structure. The energy absorbed by the buoyant leg under different load cases is shown in Fig. 11.

Table 4 Impact analysis results

Case	Peak force (MN)	Shell Deformation (m)	Maximum Energy absorbed (MJ)
Case 1	2.189	0.208	0.392
Case 2	4.123	0.420	1.568
Case 3	6.519	0.587	3.532
Case 4	8.823	0.758	6.279

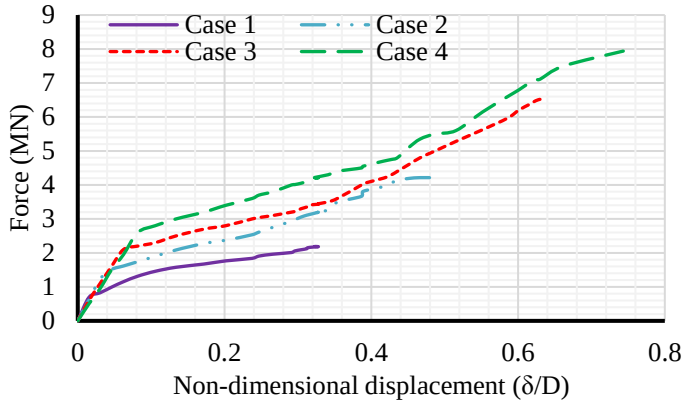

Fig. 10 Load versus non-dimensional displacement curve

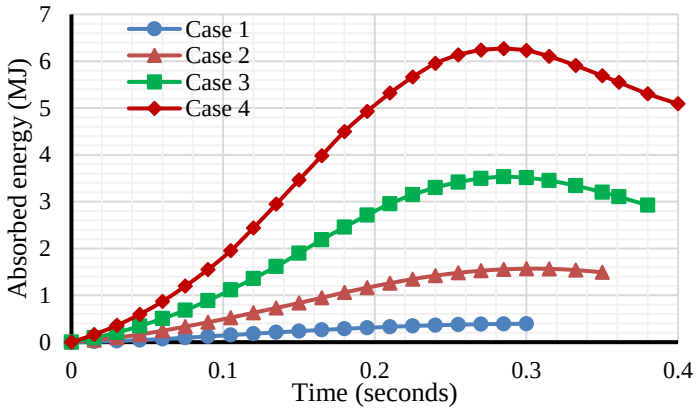

Fig. 11 Energy absorbed by buoyant leg

7. Response of triceratops

Assessment of post-impact response of triceratops is very important to find the tether tension variation under high lateral displacement of one buoyant leg. The structure should be designed in such a way that the accidental collisions does not cause complete collapse or capsizing of the platform. The structure should be able to withstand the environmental loads even after accidents. In addition, the structure should also be able to withstand flooding of any one watertight compartments in the buoyant leg after damage. Also, if the shell stiffeners are designed according to code provisions, the dent depth will not affect the external pressure resistance of the structure. However, it may result in a significant reduction in the axial load carrying capacity. Failure may be assumed to occur when the maximum stress in the undamaged shell reaches the collapse strength. Under the different impact load cases considered, the maximum stress developed in the cylindrical shell and stiffeners are well below the collapse strength, and hence under these impact conditions, the structure may not completely collapse. However, the impact loads may affect the dynamic

response of triceratops significantly. Thus, Numerical analyses are carried out to assess the dynamic response of triceratops under impact loads cases using Ansys Aqwa. The triangular deck of triceratops is modeled as a solid element with triangular and quadrilateral elements. The buoyant legs are modeled as tube elements. They are connected to the deck by three ball joints.

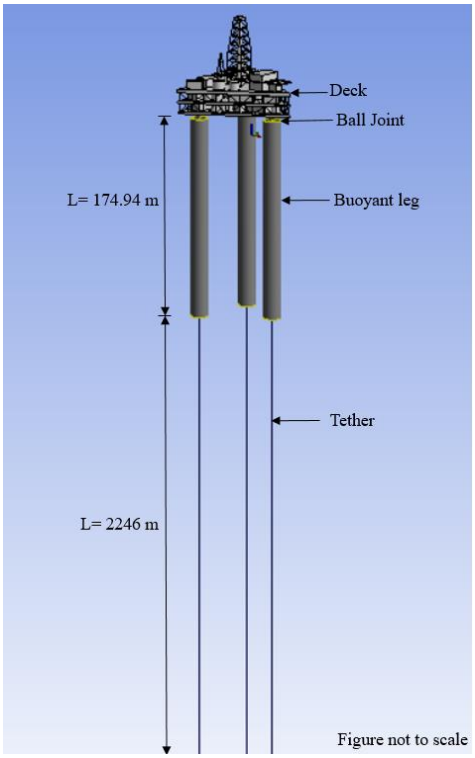

Fig. 12 A numerical model of a triceratops

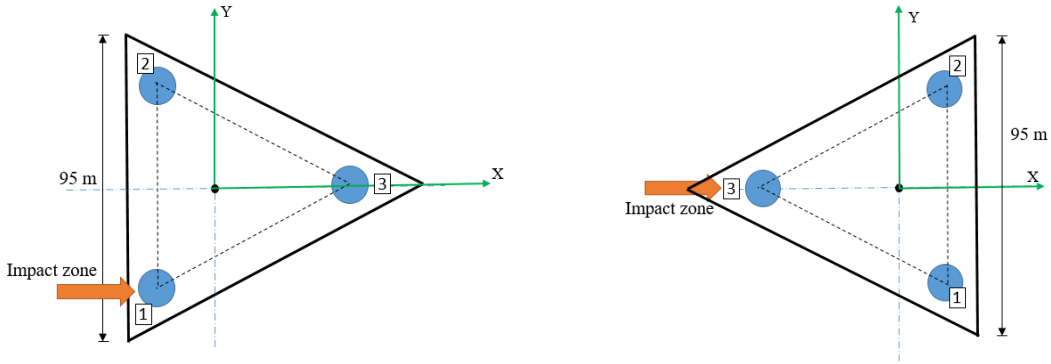

(i) Impact load on buoyant leg 1 (ii) Impact load on buoyant leg 3

Fig. 13 Collision zone for impact response analysis

The buoyant legs are position restrained by a set of taut moored tethers, modeled as linear cables. The initial pretension is applied by specifying the stiffness and unstretched length of the cable. The numerical model is shown in Fig. 12. Initially, hydrostatic analysis is carried out to check the stability of the structure, followed by time response analysis. As triceratops is a multi-legged structure, all three buoyant legs are prone to collision. Hence, impact response analyses are carried out for an accidental collision on buoyant leg 1 and buoyant leg 3, as shown in Fig. 13.

7.1 Impact on buoyant leg 1

The impact load time history obtained from the explicit analysis is applied as structure force on buoyant leg 1. The impact load on buoyant leg causes surge response in the buoyant legs as well as in the deck. As the Centre of Gravity of the buoyant leg is located near the keel, the impact load above Mean Sea Level also induces pitch response in the buoyant leg 1. However, the pitch response is not transferred to the deck due to the presence of ball joints. The responses in all other degrees of freedom are negligible. The response of the deck under impact load on buoyant leg 1 under different impact load cases are listed in Table 5. As seen from the table, the mean value of surge and pitch responses are very close to zero. Thus, the impact load does not result in the mean shift of the platform. The maximum surge and pitch responses are observed in the impacted buoyant leg.

The surge response is transferred from impacted buoyant leg to other buoyant legs through the deck. The response of the impacted buoyant leg is shown in Fig. 14. A continuously decaying surge and pitch responses are observed in both deck, and buoyant legs and the decay rate is comparatively less in the deck. Under higher impact load, significant sway responses are observed in buoyant leg 1 and buoyant leg 2, which occurs due to transverse vibration in buoyant legs and deck. Tethers are the crucial components in compliant platforms like a triceratops. Hence, the tether tension analysis. It is observed that the difference in tether tension response of tethers in three buoyant legs is insignificant. The results of tether tension analysis in buoyant leg1 for different load cases are given in Table 6. The tether tension variation is less than 3% under impact load action.

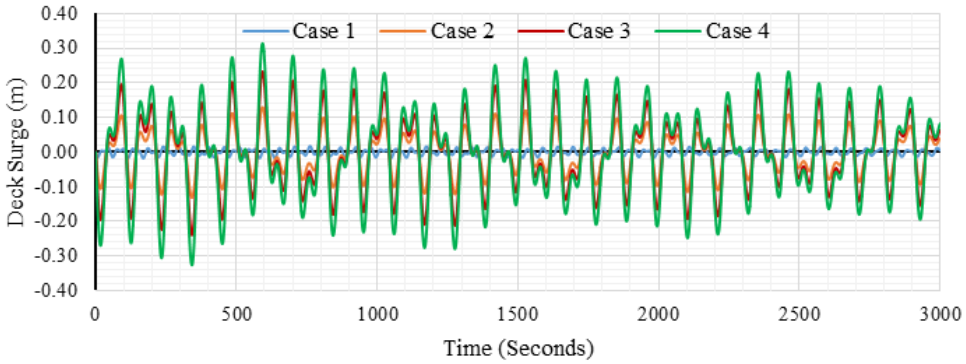

Fig. 14 Surge response in impacted buoyant leg 1

Table 5 Response of triceratops under impact load on buoyant leg 1

Load case	Degrees of freedom		Deck	Buoyant leg 1	Buoyant leg 2	Buoyant leg 3
Case 1	Surge (m)	Maximum	0.015	0.018	0.008	0.012
		Minimum	-0.015	-0.018	-0.008	-0.012
	Pitch (deg)	Maximum	0.001	0.018	0.013	0.011
		Minimum	-0.001	-0.018	-0.013	-0.011
Case 2	Surge (m)	Maximum	0.104	0.129	0.048	0.087
		Minimum	-0.102	-0.131	-0.048	-0.091
	Pitch (deg)	Maximum	0.003	0.125	0.074	0.079
		Minimum	-0.003	-0.122	-0.072	-0.077
Case 3	Surge (m)	Maximum	0.155	0.233	0.078	0.155
		Minimum	-0.166	-0.239	-0.076	-0.166
	Pitch (deg)	Maximum	0.145	0.230	0.117	0.145
		Minimum	-0.138	-0.219	-0.116	-0.138
Case 4	Surge (m)	Maximum	0.263	0.314	0.097	0.209
		Minimum	-0.255	-0.326	-0.095	-0.227
	Pitch (deg)	Maximum	0.004	0.316	0.145	0.199
		Minimum	-0.003	-0.295	-0.144	-0.187

Table 6 Tether tension analysis of buoyant leg 1 tether

Load case	Maximum tension (MN)	Minimum Tension (MN)	Tether tension variation (%)
Case 1	27.91	27.43	0.97
Case 2	28.29	27.05	2.33
Case 3	28.18	27.11	1.95
Case 4	28.29	27	2.33

7.2 Impact on buoyant leg 3

The impact load on buoyant leg 3 also causes periodic oscillation of deck in surge degrees of freedom, and the response of buoyant leg 3 is shown in Fig. 15. The surge response gets transferred from impacted buoyant leg to other buoyant legs through the deck. After the initial impact, the deck and buoyant legs start oscillating about its mean position. The responses increase with the increase in the impact load. The responses in non-impacted buoyant legs are almost similar, as seen in Table 7. The tether tension variation increases with the increase in the impact velocity and duration, as seen in Table 8. The responses of the deck and buoyant legs in the surge and pitch degrees of freedom under the action of impact load on buoyant leg 1 and buoyant leg 3 shows slight variation. However, increased tether tension variation is seen in the tethers of buoyant leg 3 under the impact. It occurs due to the asymmetry in the geometric configuration of the platform. Thus, in addition to the duration of impact and maximum impact force, the structural

geometry and collision zone location also plays a significant role in deciding the response of triceratops under impact action.

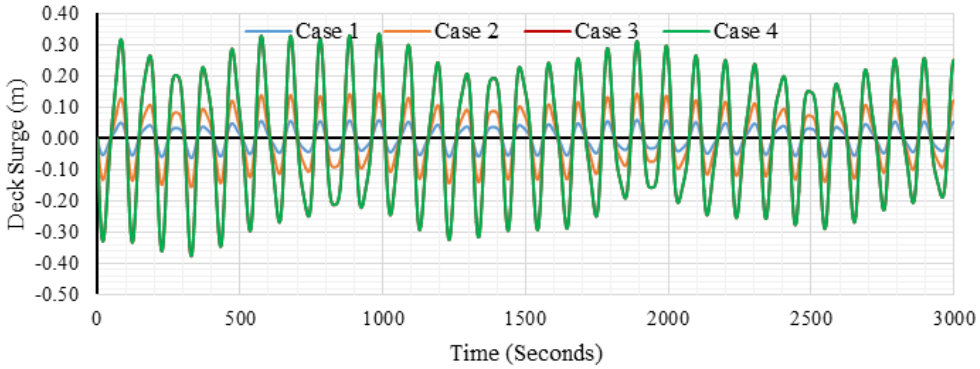

Fig. 15 Surge response in impacted buoyant leg 3

Table 7 Response of triceratops under impact load on buoyant leg 3

Load case	Degrees of freedom		Deck	Buoyant leg 1	Buoyant leg 2	Buoyant leg 3
Case 1	Surge (m)	Maximum	0.042	0.036	0.037	0.060
		Minimum	-0.041	-0.038	-0.038	-0.062
	Pitch (deg)	Maximum	0.003	0.032	0.032	0.042
		Minimum	-0.003	-0.031	-0.031	-0.041
Case 2	Surge (m)	Maximum	0.105	0.089	0.089	0.145
		Minimum	-0.104	-0.094	-0.094	-0.155
	Pitch (deg)	Maximum	0.002	0.079	0.079	0.105
		Minimum	-0.002	-0.078	-0.078	-0.102
Case 3	Surge (m)	Maximum	0.192	0.157	0.157	0.256
		Minimum	-0.189	-0.171	-0.172	-0.281
	Pitch (deg)	Maximum	0.003	0.145	0.145	0.191
		Minimum	-0.003	-0.139	-0.139	-0.183
Case 4	Surge (m)	Maximum	0.260	0.207	0.206	0.335
		Minimum	-0.253	-0.230	-0.229	-0.376
	Pitch (deg)	Maximum	0.003	0.195	0.195	0.257
		Minimum	-0.004	-0.184	-0.184	-0.242

Table 8 Tether tension analysis of buoyant leg 3 tether

Load case	Maximum tension (MN)	Minimum Tension (MN)	Tether tension variation (%)
Case 1	29.05	28.18	5.64
Case 2	29.15	28.24	5.64
Case 3	29.37	28.02	6.22
Case 4	29.38	28.05	6.23

Table 9 Effect of strain rate hardening

Case	Strain rate (/s)	Peak force (MN)	Shell Deformation (m)	Maximum Energy absorbed (MJ)
Case 1	25	2.222	0.228	0.392
	50	2.224	0.229	0.392
	100	2.225	0.229	0.392
Case 2	25	4.281	0.412	1.570
	50	4.310	0.412	1.570
	100	4.310	0.415	1.570
Case 3	25	6.689	0.571	3.521
	50	6.712	0.571	3.521
	100	6.757	0.573	3.528
Case 4	25	9.075	0.730	6.263
	50	9.125	0.730	6.268
	100	9.167	0.731	6.273

8. Effect of strain rate hardening

For more accurate prediction of impact response, consideration of strain rate effect becomes imperative. Numerical studies are also carried out by varying the strain rate effect under different impact load cases. Material properties, as discussed in Fig. 4, are included to account for the strain rate effect in the analysis. It is seen that the effect strain hardening reduces with the increase in the strain rate. Hence, strain rates of 25/s, 50/s, and 100/s are considered for the parametric study, and the results are tabulated in Table 9. From the results, it is observed that the effect of strain rate on impact response of buoyant leg is very less. The change in the impact response under higher strain rates is negligible. It is also noted that the strain rate effect increases the maximum force on the buoyant leg at higher impact durations. The peak force and the maximum shell deformation increases with the increase in the strain rate, the variation in magnitude being very small. Since the variation in the peak force is very less under different cases considered, the response of deck and buoyant legs of triceratops are also not affected by the change in strain rate.

9. Conclusions

This study aims at investigating the impact response of the buoyant leg of a triceratops. The buoyant legs are designed as orthogonally stiffened cylindrical shells with stringers and ring frames. The impact analysis is carried out on a single buoyant leg with a rectangularly shaped indenter. From the impact load time history obtained, the hydrodynamic response analysis of triceratops is carried out. The shell deformation increases with the increase in the impact duration and collision velocity. The ring stiffeners hinder the spread of plastic strain longitudinally. The stringer stiffeners undergo large deformation in the contact area. The plastic strain in cylindrical shell and stiffeners is seen only at the impact location. In addition to local weakening of buoyant leg, the impact loads also cause continuous periodic vibration in the deck and buoyant legs in the surge and pitch degrees of freedom. As tethers are the crucial components in triceratops, the failure of the tether may eventually lead to a collapse of the structure. The tether tension variation under different impact load cases is less than 2% when the impact load acts on the buoyant leg located on the broader side of triceratops (in buoyant leg 1). Higher tether tension variation is observed when the impact load acts on the buoyant leg location on the pointed end of the deck (buoyant leg 3), which is mainly due to the unsymmetrical geometric configuration of the deck. The impact response of buoyant leg with varying strain rate effect shows significant variation in impact load at higher impact durations. However, very small variation is observed in the response of triceratops under varying strain rate effect.

References

Amdahl, J. and Eberg, E. (1993), "Ship collision with offshore structures", *Proceedings of the 2nd European Conference on Structural Dynamics (EURODYN'93), Trondheim, Norway, June*.

Cerik, B.C., Shin, H.K. and Cho, S.R. (2015), "On the resistance of steel ring-stiffened cylinders subjected to low-velocity mass impact", *Int. J. Impact Eng.*, **84**, 108-123.

Chandrasekaran, S. and Nagavinothini, R. (2018), "Dynamic analyses and preliminary design of offshore triceratops in ultra-deep waters", *Innov. Infrastruct. Solutions*, **3**(1), 16.

Chandrasekaran, S. and Nagavinothini, R. (2018), "Tether analyses of offshore triceratops under the wind, wave, and current", *Mar. Syst. Ocean Technol.*, **13**(1), 34-42.

Cho, S.R., Choi, S.I. and Son, S.K. (2015), "Dynamic material properties of marine steels under impact loadings", *Proceedings of the 2015 World Congress on Advances in Structural Engineering and Mechanics,* ASEM15. Incheon, Korea.

Do, Q.T., Muttaqie, T., Shin, H.K. and Cho, S.R. (2018), "Dynamic lateral mass impact on steel stringer-stiffened cylinders", *Int. J. Impact Eng.*, **116**, 105-126.

Feng, Y., Li, H., Li, C., Ruan, J., Zhang, Q. and Xu, W. (2017), "Investigation on the Structure Strength and Stability of Ring-Stiffened Cylindrical Shell With Long Compartment and Large Stiffener", *Proceedings of the ASME 2017 36th International Conference on Ocean, Offshore and Arctic Engineering* (pp. V03BT02A034-V03BT02A034). American Society of Mechanical Engineers.

Jin, W.L., Song, J., Gong, S.F. and Lu, Y. (2005), "Evaluation of damage to offshore platform structures due to the collision of the large barge", *Eng. Struct.*, **27**(9), 1317-1326.

Karroum, C.G., Reid, S.R. and Li, S. (2007), "Indentation of ring-stiffened cylinders by wedge-shaped indenters—Part 1: An experimental and finite element investigation", *Int. J. Mech. Sci.*, **49**(1), 13-38.

Khedmati, M.R. and Nazari, M. (2012), "A numerical investigation into the strength and deformation characteristics of preloaded tubular members under lateral impact loads", *Mar. Struct.*, **25**(1), 33-57.

Kvitrud, A. (2011), "Collisions between platforms and ships in Norway in the period 2001-2010", *Proceedings of the ASME 2011 30th International Conference on Ocean, Offshore and Arctic Engineering* (637-641). American Society of Mechanical Engineers.

Liapis, S., Bhat, S., Caracostis, C., Webb, C., Lohr, C. (2010), Global performance of the Perdido spar in waves, wind, and current–numerical predictions and comparison with experiments. OMAE2010-2116.

Nagavinothini, R. and Chandrasekaran, S. (2019), "Dynamic response analyses of offshore triceratops in ultra-deep waters under the wind, wave, and current", *Structures*, **20**, 279-289. DOI: 10.1016/j.struc.2019.04.009.

Ronalds, B.F. and Dowling, P.J. (1988), "Collision resistance of orthogonally stiffened shell structures", *J. Constr. Steel Res.*, **9**(3), 179-194.

Singh, N.K., Cadoni, E., Singha, M.K. and Gupta, N.K. (2011), "Dynamic tensile behavior of multiphase high yield strength steel", *Mater. Design*, **32**(10), 5091-5098.

Srinivasan, C. and Nagavinothini, R. (2017), "Analysis and Design of Offshore Triceratops under Ultra-Deep Waters", *World Academy of Science, Engineering and Technology, International Journal of Structural and Construction Engineering*, *4*(11).

Srinivasan, C. and Nagavinothini, R. (2019a), "The ice-induced response of offshore triceratops", *Ocean Eng.*, **180**, 71-96. DOI: 10.1016/j.oceaneng.2019.03.063.

Srinivasan, C. and Nagavinothini, R. (2019b), "Tether analyses of offshore triceratops under ice loads due to continuous crushing", *Intl. J. Innov. Infrastruct. Solutions*, 4:25. DOI: 10.1007/s41062-019-0212-5.

Standard, N.O.R.S.O.K. (2007), N-003. *Actions and Action Effects, Rev. 1*.

Storheim, M. and Amdahl, J. (2014), "Design of offshore structures against accidental ship collisions", *Mar. Struct.*, **37**, 135-172.

Syngellakis, S. and Balaji, R. (1989), "Tension leg platform response to impact forces", *Marine Struct.*, **2**(2), 151-171.

Veritas, D.N. (2010), Buckling strength of shells, recommended practice DNV-RP-C202. *Det. Nor. Ver. Class. AS, Veritasveien*, *1*.

White, C.N., Copple, R.W. and Capanoglu, C. (2005), "Triceratops: an effective platform for developing oil and gas fields in deep and ultra-deepwater", *Proceedings of the 15th International Offshore and Polar Engineering Conference*. International Society of Offshore and Polar Engineers.

MK